SPACE SCIENCES

Early oxidation of the martian crust triggered by impacts

Zhengbin Deng[1]*[†], Frédéric Moynier[1], Johan Villeneuve[2], Ninna K. Jensen[3], Deze Liu[1], Pierre Cartigny[1], Takashi Mikouchi[4], Julien Siebert[1], Arnaud Agranier[5], Marc Chaussidon[1], Martin Bizzarro[1,3]

Despite the abundant geomorphological evidence for surface liquid water on Mars during the Noachian epoch (>3.7 billion years ago), attaining a warm climate to sustain liquid water on Mars at the period of the faint young Sun is a long-standing question. Here, we show that melts of ancient mafic clasts from a martian regolith meteorite, NWA 7533, experienced substantial Fe-Ti oxide fractionation. This implies early, impact-induced, oxidation events that increased by five to six orders of magnitude the oxygen fugacity of impact melts from remelting of the crust. Oxygen isotopic compositions of sequentially crystallized phases from the clasts show that progressive oxidation was due to interaction with an ^{17}O-rich water reservoir. Such an early oxidation of the crust by impacts in the presence of water may have supplied greenhouse gas H_2 that caused an increase in surface temperature in a CO_2-thick atmosphere.

INTRODUCTION

The NWA 7533/7034 regolith breccia and other 15 paired meteorites contain igneous clasts with noritic, basaltic to monzonitic compositions (*1*). These clasts have been proposed to be the products of an early remelting, likely by impacts (*2–4*), of the primary crust derived from the martian mantle. Hence, these igneous clasts can provide insights into the ancient surface of Mars, allowing us to investigate the physicochemical conditions that existed at the surface of the planet, including the oxygen fugacity at the time of crustal reworking. This information is critical to constrain the timing of establishment of Mars' hydrosphere and atmosphere and, hence, the potential for early habitability. On Earth, oxidized lavas with ΔFMQ (i.e., oxygen fugacity in logarithmic deviation relative to the fayalite-magnetite-quartz buffer) values as high as +5 occur in arc systems due to the recycling into the sub-arc mantle of crustal material that experienced interactions with seawater (*5, 6*). Differentiated meteorites typically have ΔFMQ values below zero (*6*), among which martian meteorites including shergottites, nakhlites, and chassignites (i.e., SNC meteorites) are the most oxidized ones, with ΔFMQ ≈ −4 to −1 for shergottites and ≈0 for nakhlites and chassignites (*6, 7*). In contrast, some igneous clasts from the NWA 7533/7034 meteorites are reported to be highly oxidized with ΔFMQ values of up to +4 (*8, 9*), but it is unclear whether the oxidized nature of these clasts represents early magmatic or late postmagmatic processes (*8*).

Titanium isotopic variations in magmatic rocks are mainly controlled by Fe-Ti oxide crystallization (*10, 11*). Because of the different coordination numbers of Ti in Fe-Ti oxides (sixfold) and silicate melts (four-, five-, and sixfold depending on the melt composition)

(*12*), Fe-Ti oxides preferentially incorporate light Ti isotopes such that fractional crystallization of Fe-Ti oxides produces isotopically heavy residual melts (*10, 11, 13–15*). At Fe-Ti oxide saturation, Fe-Ti oxide crystallization is promoted by the decreasing solubility of total FeO (FeOtot) due to a change in either melt composition or oxygen fugacity (*16–18*). In terms of melt composition, cooling leads to crystallization of olivine or pyroxene, thereby lowering the Mg# and the FeOtot contents at Fe-Ti oxide saturation in silicate melts. Instead, an increase in oxygen fugacity leads to a decrease in the FeOtot contents but an increase in the Mg# values of the silicate melts due to fractional crystallization of Fe-Ti oxides (see equation 5 in *16*). Thus, the combination of chemical and Ti isotopic compositions can be used to determine the magmatic thermal and/or redox histories of igneous rocks, in other words, the T-fO_2 paths during magma evolution (*16*).

RESULTS AND DISCUSSION

Fifteen igneous clasts of the NWA 7533 meteorite selected from a larger set studied for petrology (12 basaltic clasts, 1 phono-tephritic clast, and 1 foiditic clast, as well as an orthopyroxene crystal; figs. S7 to S14 and data files S1 and S2) were chosen for detailed chemical and isotopic investigations. Alkali and SiO_2 contents of the studied NWA 7533 igneous clasts match with the global gamma ray spectrometry (GRS) data (*19, 20*) and the rover data of surface rocks and soils in Gusev (*21, 22*) and in Gale (*23, 24*) craters, which have higher alkali contents compared with SNC meteorites (Fig. 1) (*25, 26*). The present basaltic clasts are characterized by enrichments in light rare earth and siderophile elements, which is consistent with earlier work (fig. S1 and data file S2) (*3, 27–31*). Zircons extracted from the basaltic clast C27 yield ancient and overlapping ^{207}Pb/^{206}Pb dates, with one zircon defining nearly concordant U-Pb systematics corresponding to a ^{207}Pb/^{206}Pb age of 4443.6 ± 1.2 million years (Ma) (*32*). These data, combined with existing U-Pb systematics of zircons from the NWA 7533/7034 meteorite (*3, 30, 31, 33*), confirm the antiquity of the igneous clasts. This is in line with the interpretation that these ages reflect the remelting of the primary crust during the first 100 Ma of the planet's history (*2, 3*). Hence, the magmatic
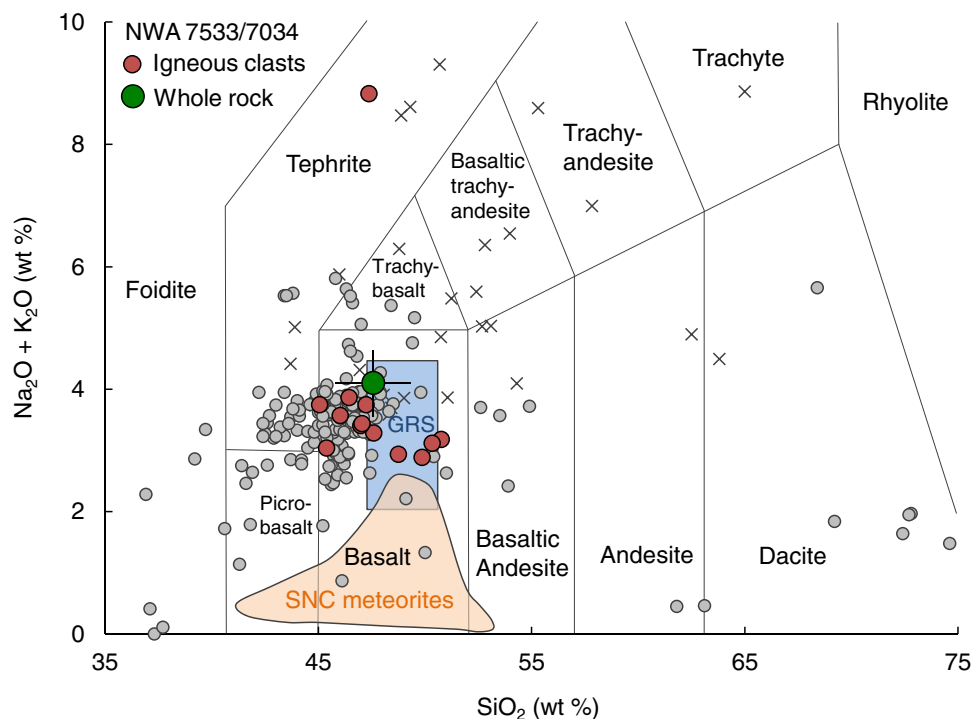
Fig. 1. Alkali (Na$_2$O + K$_2$O) versus SiO$_2$ classification diagram for volcanic rocks modified after Agee *et al.* (*4*) and McSween *et al.* (*19*). The NWA 7533 clasts in this study (the red solid circles), whole-rock NWA 7034 meteorite in Agee *et al.* (*4*) (the green solid circle), and SNC meteorites (*25*, *26*) (the orange field) are compared with the gamma-ray spectrometer (GRS) data of the Mars Odyssey orbiter (*19*, *20*) and those of rocks and soils in Gusev Crater (the gray dots) from the alpha particle x-ray spectrometer (APXS) on the Spirit Rover (*21*, *22*) and in Gale Crater (the grey crosses) from APXS (*23*) and laser-induced breakdown spectrometer (ChemCam) (*24*) on the Curiosity Rover. Note that clast C4 is plotting outside the figure due to its high alkali content (data file S1).

histories of these clasts provide insights into the processes and conditions of reworking of Mars' first crust.

The NWA 7533 igneous clasts are characterized by elevated δ^{49}Ti values ranging from +0.055 ± 0.025 per mil (‰) to +0.432 ± 0.032‰ (i.e., a delta notation of ^{49}Ti/^{47}Ti ratio relative to OL-Ti standard) at high Mg# values of 39.5 to 55.5 (Fig. 2). This is in contrast with (i) terrestrial rocks like the lavas from Agung volcano in the Sunda Arc [ΔFMQ ≈ +2.4 (*10*)] and those from Hekla volcano in Iceland [ΔFMQ ≈ +0.9 (*11*)] that became saturated in Fe-Ti oxides at low Mg# values, and (ii) magmatic meteorites like shergottites (including the most differentiated shergottite, Los Angeles) and angrites that have lower oxygen fugacity with ΔFMQ = −4 to −1 and did not ever approach Fe-Ti oxide saturation even at Mg# values as low as 23.8 (Fig. 2 and data file S1). It is unlikely that the high δ^{49}Ti values of the NWA 7533 clasts reflect contamination by chondrite-like impactors given that the various chondrite groups have δ^{49}Ti values that are within ±0.050‰ of known oxide-undersaturated mafic and ultramafic rocks (*10*, *11*, *34–36*). Thus, the observed δ^{49}Ti-Mg# systematics indicates that Fe-Ti oxide crystallization occurred during the evolution of the melts parental to NWA 7533 clasts, implying that the oxidized features of the clasts are fingerprints from early magmatic processes rather than postmagmatic resetting. Substantial Fe-Ti oxide crystallization without any systematic decrease in Mg# value suggests that the decrease in magnetite solubility in silicate melts of the clasts is mainly caused by an increase in oxygen fugacity rather than by a change in melt composition due to cooling. This interpretation is in line with the higher magmatic ΔFMQ values of +1.6 to +3.9 of these clasts relative to that of the martian mantle as

sampled by SNC meteorites (*6*) [ΔFMQ = −4 to −1; see (*12*)]. In support of our inference, we reproduced experimentally such an oxidation-induced Fe-Ti oxide removal. In our experiments, an increase in the ΔFMQ values from −2.9 to +2.6 or to +6.5 resulted in notable magnetite crystallization from Fe-rich basaltic parental melts and, therefore, decreasing FeOtot contents in the oxidized melts [see (*16*)]. The increased δ^{49}Ti values of +0.056 ± 0.025‰ to +0.160 ± 0.020‰ in nakhlites with a cumulate origin suggest that their parental magmas have also experienced fractionation of Fe-Ti oxides, which is consistent with the more oxidized nature of these meteorites relative to shergottites (*6*, *7*). Considering that some of the studied clasts date back to 4443.6 ± 1.2 Ma (*32*), oxidation of the parental magmas of these igneous clasts by up to six orders of magnitude requires an oxidizing agent, likely water, at the surface of the planet at the time of reworking of the crust.

Taking a conservative approach and assuming that the clasts' crustal precursors likely had ΔFMQ values and FeOtot contents close to those of shergottites (i.e., at equilibrium with the martian mantle), progressive oxidation of the magmas generated by melting of the primary crust will result in fractional crystallization of Fe-Ti oxides. This magnetite fractionation scenario is in agreement with the correlated decrease in the concentration of FeOtot and that of elements compatible in magnetite, namely, Ni, V, Co, and some highly siderophile elements like Ir, Rh, Ru, and Os (with Pt as an exception due to its low partition coefficient between magnetite and silicate melt under oxidized conditions) (Fig. 3 and fig. S2) (*37*). Combined V-Fe systematics in these igneous clasts implies on average a low partition coefficient of ~2.5 for V between Fe-Ti oxides
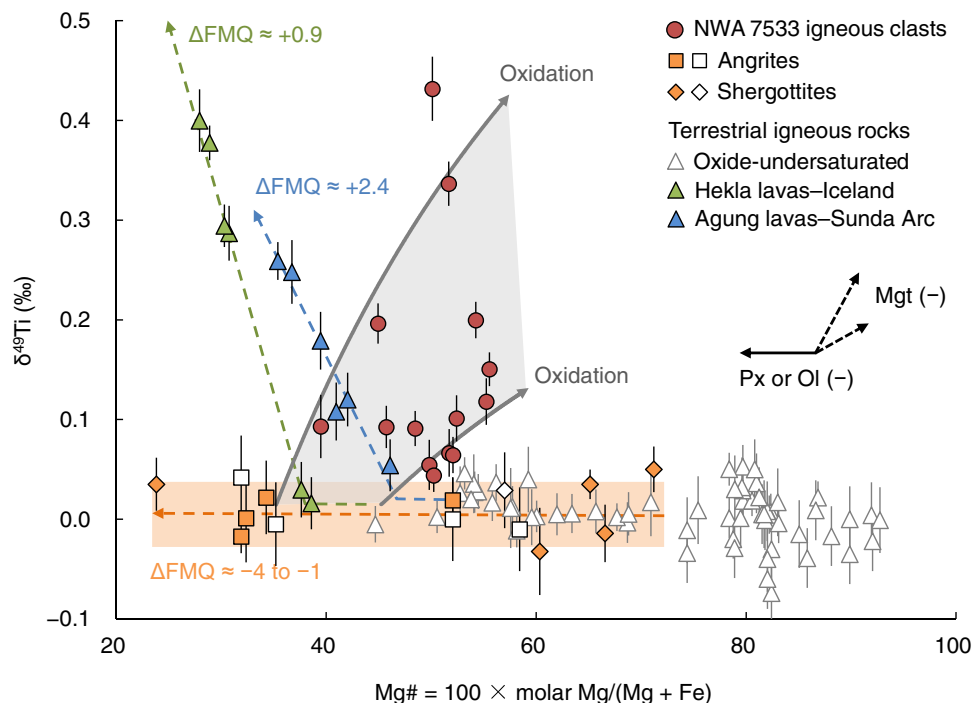
Fig. 2. Plot of δ^{49}Ti versus Mg# for the NWA 7533 igneous clasts, shergottites, angrites, and terrestrial igneous rocks. Data of the terrestrial oxide-undersaturated rocks are from Millet *et al.* (*10*), Greber *et al.* (*34*), and Deng *et al.* (*35*). Terrestrial differentiated rocks with ΔFMQ values of $\approx$+0.9 [Hekla lavas, Iceland; (*11*)] and $\approx$+2.4 [Agung lavas, Sunda Arc; (*10*)] follow different paths controlled by the change of composition due to cooling of magmas, relative to that of shergottites and angrites with ΔFMQ values of $\approx$−4 to −1. The data for angrites and shergottites from this study are shown by orange squares and diamonds, respectively, with those from Greber *et al.* (*34*) represented by white squares and diamonds (data file S1). The two gray curves describe the effects of oxidation to ΔFMQ = +3 to 4 on the shergottitic melts at ΔFMQ $\leq$−2.5 with Mg# values of 35 and 45, respectively [see (*16*)]. The black arrows represent the controls on the melt δ^{49}Ti and Mg# values from removal of pyroxene (Px) or olivine (Ol) (the solid arrow), or of magnetite (Mgt) (the dashed arrows).

and melts, which independently confirms the oxidized nature of the equivalent magmas (ΔFMQ $\geq$ +3) based on the calibrations in *38*. The basaltic clasts with the least magnetite fractionation (e.g., clast C3) have high Ni and Ir concentrations of $\approx$1500 parts per million (ppm) and $\approx$80 parts per billion (ppb) [this study and (*3*)], respectively. Assuming Ni $\approx$ 150 ppm and Ir $\approx$ 0 ppb for the reduced primary crust derived from martian mantle (*25*), and Ni $\approx$ 10,500 ppm and Ir $\approx$ 455 ppb for the chondritic impactor (*39*), the high Ni and Ir concentrations in the NWA 7533/7034 igneous clasts (Fig. 3) require the addition of ~15 weight % (wt %) of chondritic material to their parent magmas, which is higher than the values estimated directly from the apparent Ni and Ir contents of the bulk clasts (~3 to 5 wt %) (*3*, *4*, *27*, *28*). The various enrichments in Ni observed for rocks and soils in Gusev and Gale craters suggest that addition of Ni to the primary crust of Mars by impacts was likely a general process (Fig. 3). Tracking ferrous-ferric iron budgets in the melts over oxidation shows that 2.4 to 2.9% of total oxygen in the oxidized melts of the clasts would originate from the oxidant (*16*), corresponding to a consumption of 1.2 to 1.4 wt % water.

Such an oxidation scenario for the origin of the NWA 7533/7034 igneous clasts is corroborated by their triple O isotope compositions, from both this study and literature (*4*, *40*). In detail, a pyroxene crystal (i.e., P3 from this study) and a pyroxene separate [in (*40*)] have Δ^{17}O values (+0.27 ± 0.05‰ and +0.33‰, n = 1, respectively) within experimental error identical to that of SNC meteorites (Δ^{17}O = +0.318 ± 0.016‰, 2 SD, n = 56) (*41*). This confirms that the crustal precursors of the NWA 7533/7034 igneous clasts likely derive from

a martian mantle reservoir with Δ^{17}O value similar to that of SNC meteorites, in line with the petrological and chemical constraints. Note that our samples were analyzed only once and, hence, the resulting errors are comparatively large. Yet, Δ^{17}O values different from other SNC meteorites are identified for two clast samples (C16 and C17) having values of ~0.4‰. These values in the NWA 7533 igneous clasts are inconsistent with the concept of Δ^{17}O homogeneity of differentiated bodies. These O-isotope data require a late partial exchange of oxygen between the parent melts of the basaltic clasts and oxidizer having a distinctively high Δ^{17}O value to explain the higher bulk clast Δ^{17}O values and the dependence of maximal Δ^{17}O values of minerals with the order of magnetite $\leq$ pyroxene $\leq$ apatite $\leq$ plagioclase $\leq$ zircon $\leq$ K-feldspar for six studied holocrystalline clasts (i.e., C11, C16, C4, C7, C18, and C27) (Fig. 4, fig. S3, and data file S3). It is also noteworthy that the magnetite, pyroxene, and plagioclase phenocrysts have systematically lower maximal Δ^{17}O values than those making the groundmass (Fig. 4). As proposed by Nemchin *et al.* (*42*), the Δ^{17}O variability in the ~4.43–billion year (Ga)–old zircons from the NWA 7533 meteorite can result either from an early (~4.43 Ga) assimilation of a high-Δ^{17}O component into the parental magmas of the clasts or, alternatively, from a late (~1.7 Ga) oxygen exchange between the minerals in the clasts and a hydrothermal fluid with high Δ^{17}O values. Our Δ^{17}O data for minerals of various types and textures allow us to differentiate between the two models. Under hydrothermal conditions, oxygen diffuses much faster in feldspar and apatite than in magnetite, pyroxene, and zircon (*43*), and therefore, feldspar and apatite are predicted to
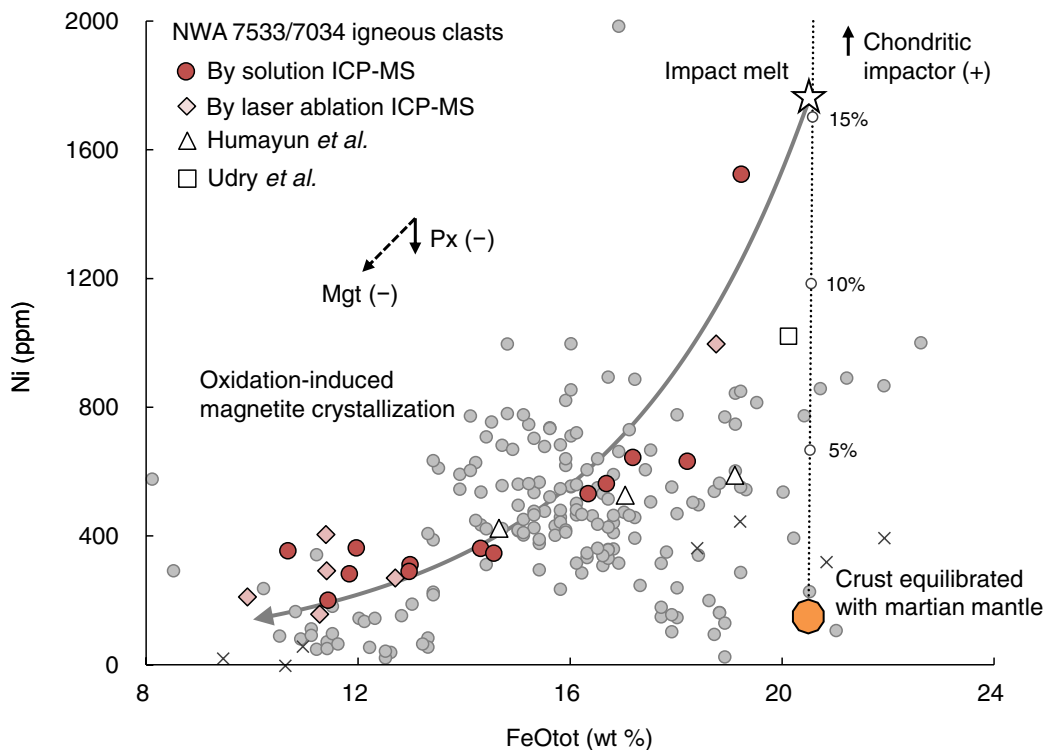
Fig. 3. Plot of Ni concentration versus total FeO (FeOtot) for the NWA 7533 igneous clasts. The primary crust at equilibrium with martian mantle has been assumed to have Ni ≈ 150 ppm and FeOtot ≈ 20.5 wt % at an average MgO content of 8 wt %, based on the Ni versus FeOtot systematics from SNC meteorites (*25, 26*). High Ni concentrations in the NWA 7034/7533 igneous clasts (data file S2) would require addition of chondritic material with Ni ≈ 10,500 ppm and FeOtot ≈ 21.0 wt % (*39*). The gray curve represents the incremental effects of Fe-Ti oxide removal (with an assumed partition coefficient of 13 for Ni between magnetite and melt) caused by an oxidation of impact melts due to mixing between the primary crust and a chondritic impactor (shown by the dotted line with 5% increments). The arrows show the controls from fractional crystallization of pyroxene (Px) (the solid arrow) and magnetite (the dashed arrows). Data of the NWA 7533/7034 igneous clasts in Humayun *et al.* (*3*) (the triangles) and Udry *et al.* (*27*) (the square) and those of rocks and soils in Gusev Crater [the gray dots (*21, 22*)] and in Gale Crater [the gray crosses (*23*)] from the APXS on the Spirit and Curiosity Rovers are also shown for comparison.

reach oxygen isotopic equilibrium with the fluid much earlier than zircon and pyroxene. The mineralogical control on $\Delta^{17}O$ depicted in Fig. 4 is not consistent with this prediction, thereby supporting a progressive input of high-$\Delta^{17}O$ material during early (~4.43 Ga) magmatic processes as an explanation for the $\Delta^{17}O$ variability in the NWA 7533/7034 basaltic clasts. This is in agreement with the observation that heat-released water from the NWA 7034 meteorite, which likely reflects late-stage hydrothermal fluids, has an SNC meteorite–like $\Delta^{17}O$ value of +0.330 ± 0.011‰ (*4*) rather than an elevated $\Delta^{17}O$ composition. The addition of heavy oxygen into the parental melts, as inferred from the mineral O-isotope data, is indicative of interaction with a high-$\Delta^{17}O$ oxidant (i.e., oxidation), which, as described above, also results in magnetite crystallization. Using a $\Delta^{17}O$ value of +2.6‰ for the composition of the oxidant (Fig. 4), and a basaltic magma having initially a martian mantle–like $\Delta^{17}O$ value (+0.318‰) (*41*) and ΔFMQ ≤−2.5, an increase in ΔFMQ to +2 to 4 (i.e., 2.4 to 2.9% oxygen from oxidant) would lead to a 0.054 to 0.066‰ increase in melt $\Delta^{17}O$ [see (*16*)]. This is consistent with the shift in bulk $\Delta^{17}O$ observed for three oxidized clasts (i.e., C16, C7, and C27; $\Delta^{17}O$ = +0.383 ± 0.042‰; Fig. 4 and data file S4). Thus, our data establish that a water reservoir (either liquid or ice) characterized by a $\Delta^{17}O$ value ~2‰ higher than the martian mantle was present at the surface of the planet by ~4.44 Ga. We infer that interaction of magmas produced during

reworking of the crust with this reservoir is responsible for the $\Delta^{17}O$ variability observed in ancient igneous components on Mars.

The high-$\Delta^{17}O$ water component on early Mars may represent either water delivered by impacting material such as water-rich asteroidal bodies (*44*) or, alternatively, water equilibrating with photochemical products from the early martian atmosphere (*4, 42, 45*). Our data cannot discriminate between these two possibilities. Nonetheless, an impact origin for the NWA 7533/7034 basaltic clasts is established from their enrichment in highly siderophile elements. This interpretation is consistent with recent seismic observations indicating that the first 8 to 11 km of the martian crust is intensely fractured (*46*). It has been proposed that such early bombardment episodes may have induced elevated surface temperatures on Mars, resulting in a warm and wet early climate that is implied by the ancient records of fluvial activity (*47, 48*). However, the heat flux solely resulting from impacting bodies as large as 100 km in diameter can only induce transient warm periods lasting years on the martian surface (*47*), which is too short-lived to account for the geological evidence for long-lived fluvial activity [hundreds of million years (*49*)]. In contrast, the reducing greenhouse gases CH_4 and H_2 emitted during impact-induced remelting and oxidation of the primary crust may strongly modify the composition of the martian atmosphere, leading to a warm climate on early Mars that can potentially be sustained for millions of years (*50, 51*). As a conservative
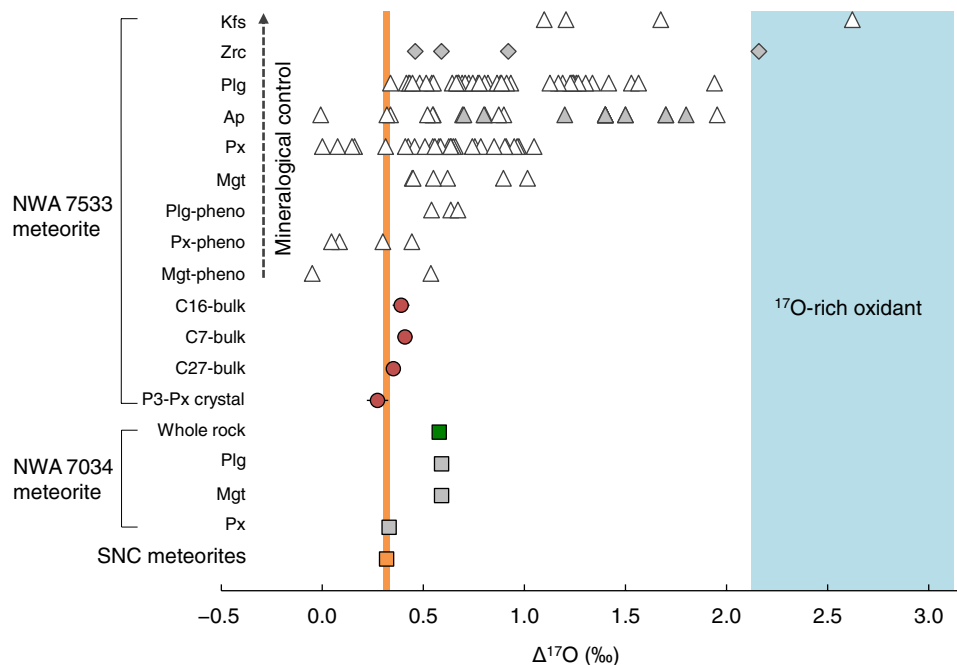
Fig. 4. Plot showing the $\Delta^{17}O$ variability of SNC meteorites and NWA 7533/7034 meteorites. The $\Delta^{17}O$ value of +0.318‰ for SNC meteorites anchored by the orange column is from Ali *et al.* (*41*), and those of whole-rock aliquot and the mineral separates of the NWA 7034 meteorite are from Agee *et al.* (*4*) and Ziegler *et al.* (*40*), respectively. Also shown are the $\Delta^{17}O$ values of components from the NWA 7533 meteorite, including one pyroxene crystal (i.e., P3) and three basaltic clasts (i.e., C16, C7, and C27) measured by laser fluorination (±0.03 to 0.05‰, 1 SD; data file S4), and those analyzed by secondary ion mass spectrometry (SIMS; ± 0.5‰, 2 SD; data file S3) for minerals in six well-crystallized clasts (C11, C16, C4, C7, C18, and C27) in this study (the white triangles), as well as zircons from Nemchin *et al.* (*42*) (the gray diamonds) and apatites from Bellucci *et al.* (*45*) (the gray triangles), The in situ data have been aligned following a mineralogical control: phenocrysts (pheno), magnetite (Mgt), pyroxene (Px), apatite (Ap), plagioclase (Plg), zircon (Zrc), and K-feldspar (Kfs). Note that the highest $\Delta^{17}O$ value from SIMS measurements on K-feldspar (i.e., +2.6 ± 0.5‰) has been assumed to represent that of the ^{17}O-rich oxidant (the light blue field).

estimate, we consider the effect of a single crustal remelting event associated with a 100-km-diameter impactor of chondritic composition, which would result in the remelting of a crustal reservoir of ~1.6 × 10^{19} kg for an impact melt–to–impactor volume ratio of ~10. Using the NWA 7533/7034 igneous clasts as a proxy for the level of oxidation of the primary crust [i.e., ~1.2 to 1.4 wt % water consumption (*16*)], this would result in the consumption of ~2 × 10^{17} kg H_2O and release ~6 mole % H_2 in a 2-bar martian atmosphere, which is enough to raise the surface temperature by ~60°C (*51*). In addition to this supply of H_2, there can be also other sources of H_2 on early Mars, e.g., Fe oxidation by H_2O in the impact vapor plumes (*48*) or degassing from volcanism (*50*). Integrating these potential supplies of H_2 predicts that a high amount of H_2 can accumulate in the martian atmosphere. This could raise the surface temperature of early Mars above the freezing point of water for several or tens of millions of years (or even longer) despite the faint young Sun (*48*, *50–53*), therefore making the early habitability of the planet possible.

MATERIALS AND METHODS
Scanning electron microprobe and quadrupole inductively coupled plasma mass spectrometer

The NWA 7533 hand specimens were cut into ≈1.3-mm-thick sections with a diamond wire saw at the Centre for Star and Planet Formation, University of Copenhagen. For the large igneous clasts showing up in at least two sections, the igneous clasts of interest were extracted from one of the sections and mounted into epoxy for

in situ chemical and isotopic characterization, and the counterpart section was then used for destructive sampling. All the studied clasts were first characterized for petrology by scanning electron microprobe (SEM) at the Institut de Physique du Globe de Paris (IPGP) (figs. S7 to S14). For a well-polished and flat sample surface, SEM can provide major element compositions for the sample that are reliable in a sub–weight percent uncertainty, as corroborated by the results from basaltic glass BHVO-2G (data files S2 and S5). The mapped igneous clasts were sampled by a microdrilling instrument at IPGP applying a tungsten carbide bit of 200 μm in diameter, and Mille-Q H_2O and pipette were used to transport the sample powders into precleaned Savillex beakers. The powders of the NWA 7533 igneous clasts and angrites, as well those of shergottites, nakhlites, and chassignites (SNC meteorites), were digested via a protocol using 26 M HF and 16 M HNO_3 acids (2:1 in volume) or/and an NaOH fusion method described in Deng *et al.* (*36*). With respect to NaOH fusion, ~10 mg of sample powder for each sample was weighed into an Ag crucible with the addition of ~200 mg of NaOH pellets (99.99% trace metal basis, Sigma-Aldrich Company) and was fused at 720°C in a furnace for 15 min, after which the sample was dissolved in ~1 M HNO_3. For the digestions with HF and HNO_3 acids, the samples were heated in 6 M HCl at 135°C for 3 days to decompose the fluorides forming from HF dissolution. For the NWA 7533 igneous clasts, an aliquot containing 5% dissolved material of each sample was dried down and dissolved in 0.5 N HNO_3 for major and trace element measurements on the Agilent quadrupole inductively coupled plasma mass spectrometer (Q-ICP-MS) at

IPGP. Helium gas (5 ml/min) was used to remove the molecular interferences in a collision-reaction interface. Scandium and indium solutions were mixed inline with sample solutions and applied as internal standards to correct for matrix effects and signal drift. Standard solutions with concentrations spanning those of sample solutions were prepared from mixing certified standards and were used to generate calibration lines between count measurements and concentrations. To overcome yield effects, MgO contents from SEM mapping were used as an internal normalization standard to return the Q-ICP-MS data into element concentrations in the individual clasts. The SiO_2 contents from SEM were also adopted, as silicon of samples was lost as SiF_4 during HF digestion. Over the whole analytical session, the composition of BHVO-2 was measured three times as unknown, and the comparison of the measured values and certified values suggests an external reproducibility of ≤5% for most elements (data file S2).

Laser ablation–high-resolution–ICP-MS

The igneous clasts showing up in at least two sections were measured for major and trace element compositions by laser ablation (LA)–ICP-MS at the Institut Universitaire Européen de la Mer (Brest), which couples a Coherent COMPex 102 Laser Ablation System (193-nm wavelength), with an Element XR high-resolution (HR)–ICP-MS. Multiple ablation spots of 160 μm in diameter were conducted on the clasts with a laser energy output of 10 J/cm^2 and a repetition rate of 10 Hz. The generated aerosols were transported by He gas into HR-ICP-MS, before which the sample aerosols were mixed with Ar gas. The analysis on each ablation spot contained 40 cycles with 3.2 s per cycle (i.e., ~1280 laser pulses), making a spot of ~150 μm in depth. The typical washout time was less than 10 s, and a pause time of 1.5 to 2 min between two analyses was applied to minimize memory effects. Data reduction on each spot was conducted by integrating the cycles except for the transient cycles at the beginning of ablation. For each igneous clast, intensity signals of all the spots were integrated, and MgO content of each clast by SEM was used as an internal normalization standard to overcome yield effects from ablation. The composition of the basaltic glasses BCR-2G, BHVO-2G, and BIR-1G was analyzed at the beginning and at the end of each session to generate calibration lines for the elements of interest, and three to four analyses on BHVO-2G inside the session confirmed that these calibration lines were stable over the session. The use of BHVO-2G as an unknown sample demonstrates an external reproducibility of 5 to 10% for all the measured elements (data file S2). Overall, chemical results from LA-ICP-MS are consistent with those from solution measurements on microdrilled aliquots by Q-ICP-MS and those for major elements by SEM, confirming the representativeness of the chemical data for the studied igneous clasts (data file S2).

Multicollector (MC)–ICP-MS for stable Ti isotopic compositions

Digestion aliquots of the NWA 7533 igneous clasts, angrites, and SNC meteorites were measured for mass-dependent Ti isotopic fractionations following a protocol in Deng et al. (36). To minimize the isotopic artifacts from incomplete Ti recovery, incomplete purification of Ti from matrix elements, or instrumental mass bias, the sample solutions were mixed with proper amounts of ^{47}Ti-^{49}Ti double spike. The mixtures were heated to 100°C on the hot plate for 1 hour, after which the mixtures were dried down and dissolved in 6 M HCl at 130°C for 1 day to further equilibrate the sample with double spike.

The purification of Ti was achieved by a three-step chromatographic procedure: (i) Fe was removed through 6 M HCl elution on the columns of 1.1-cm^3 Bio-Rad AG1-X8 resin (200 to 400 meshes), (ii) matrix elements (e.g., Mg, Ca, Al, Mo, Zr, and Hf) were cleaned by 900 μl of 12 M HNO_3 washing on the columns filled with 0.2-cm^3 Eichrom DGA resin, and (iii) the remaining matrix elements were eluted with 9.5 ml of 4 M HF using again the AG1X8 columns (36). The Ti cuts were measured on a Neptune multicollector (MC)–ICP-MS at IPGP via an APEX HF desolvating nebulizer (Elemental Scientific Inc., USA) in 0.5 M HNO_3 + 0.0015 M HF. A two-step washing with 1.2 M HNO_3 + 0.0015 M HF and 0.5 M HNO_3 + 0.0015 M HF, respectively, was carried out after each analysis, and the typical background was 2 to 5 mV on $^{48}Ti^+$. The intensities on five isotopes including $^{44}Ca^+$, $^{46}Ti^+$, $^{47}Ti^+$, $^{48}Ti^+$, and $^{49}Ti^+$ were monitored simultaneously, and a medium mass resolution ($M/\Delta M \approx 5800$) was able to avoid molecular interferences (such as $^{28}Si^{16}O^+$, $^{30}Si^{16}O^+$, and $^{28}Si^{19}F^+$) after a proper alignment of intensity peaks and by measuring at the low masses of the 44, 46, and 47 mass peaks. The interferences from $^{46}Ca^+$ and $^{48}Ca^+$ on $^{46}Ti^+$ and $^{48}Ti^+$, respectively, were corrected using the $^{44}Ca^+$ intensities, during which the instrumental Ca isotopic ratios were estimated from the natural Ca isotopic ratios ($^{44}Ca/^{46}Ca = 657.03$ and $^{44}Ca/^{48}Ca = 11.14$) by assuming a similar instrumental mass bias for Ca as that for Ti. This correction of Ca isobaric interferences, together with double-spike inversion to calculate Ti isotopic compositions of the samples, was implemented with an IsoSpike software developed in (54). A spiked Ti standard solution (referred as IPGP-Ti) was used as the bracketing standard for secondary normalization. The IPGP-Ti standard has a $\delta^{49}Ti = +0.140 \pm 0.011$‰ (95% confidence interval, $n = 8$) (36), where $\delta^{49}Ti$ represents per mil deviation of the $^{49}Ti/^{47}Ti$ ratio of the sample relative to the OL-Ti standard (10). Reference materials including BHVO-2, AGV-1, BIR-1, and BCR-2 were processed in parallel following the same protocols, which provide the $\delta^{49}Ti$ values well consistent with those reported previously (data file S1) (10, 11, 34–36).

Secondary ion mass spectrometry for in situ triple O isotopic measurements

Seven igneous clasts (C11, C16, C4, C7, C18, C27, and C3) were measured for triple O isotopic composition by secondary ion mass spectrometry (SIMS) using the CAMECA IMS 1270 E7 housed at Centre de Recherches Pétrographiques et Géochimiques (CRPG)–Centre National de la Recherche Scientifique (CNRS). The epoxy mounts hosting the samples were coated with gold and degassed in a vacuum chamber overnight. A ~5.5- to 6-nA Cs^+ primary ion beam of ~15 μm in diameter was used for sputtering to produce $^{16}O^-$, $^{17}O^-$, and $^{18}O^-$ ions, and the charge was compensated using an electron gun. An N_2 trap was used to maintain a high vacuum over the analytical sessions ($<4 \times 10^{-9}$ torr), which maintains a low production of $^{16}O^1H^-$. To further minimize $^{16}O^1H^-$ interference on $^{17}O^-$, a mass resolving power (MRP) of ≈10,000 was achieved on the central Faraday cup for $^{17}O^-$ analysis, and $^{16}O^-$ and $^{18}O^-$ were measured on L2 and H1 off-axis Faraday cups with MRP ≈ 5000 (slit 2). By doing that, the $^{16}O^1H^+$ tailing contribution on $^{17}O^-$ was kept negligible. Six standards (San Carlos olivine, KL2-G basaltic glass, Miyake anorthite, GoldEns enstatite, JV1 diopside, and BHVO-2G basaltic glass) were used to generate the instrumental mass fractionation (IMF) line at the beginning and the end of each analytical session, and three of the standards (San Carlos olivine, JV1 diopside, and BHVO-2G) were inserted into the epoxy mounts hosting the NWA

7533/7034 igneous clasts to monitor the IMF line over the whole session. Note that all the analytical spots on the NWA 7533/7034 clasts have been provided in figs. S7 to S13. The typical intensities are ~1.7×10^9 to 2.3×10^9 counts per second (cps) on $^{16}O^-$, ~6.7×10^5 to 8.8×10^5 cps on $^{17}O^-$, and ~3.6×10^6 to 4.8×10^6 cps on $^{18}O^-$ for silicates, which are 50% higher for magnetite (data file S3). Over 1 day's measurements, there could be a 0.5‰ drift on $\Delta^{17}O$ with $\Delta^{17}O = \delta^{17}O - 0.528 \times \delta^{18}O$, where $\delta^{17}O$ and $\delta^{18}O$ represent per mil deviation of $^{17}O/^{16}O$ and $^{18}O/^{16}O$ ratios relative to those of the Standard Mean Ocean Water (SMOW). A standard-sample bracketing protocol was adopted, i.e., measuring three to five spots on San Carlos olivine within the same epoxy mounts after every six to seven spots on samples or other standards, and isotopic ratios were normalized onto the bracketing San Carlos olivine. Five standards (BHVO-2G, KL2-G, Miyake, GoldEns, and JV1) provide average $\Delta^{17}O$ values close to zero with 2 SD values of ±0.4 to 0.5‰ (for 6 to 40 duplicates; data file S3). Therefore, we consider that typical uncertainty for SIMS measurements in this study should be ±0.5‰ on the $\Delta^{17}O$ value.

Ion-ratio mass spectrometer for triple O isotopic measurements

The NWA 7533 igneous clasts were extracted from the meteorite slices with a 250-μm diamond-coated wire saw, and the matrix attached to the igneous clasts was removed with diamond-coated bits. The extracted clasts were cleaned by ultrasonication and rinsing in distilled H_2O and ethanol in steps. Milligram-size (0.939 to 1.325 mg) fragments of four extracted clasts, including three high-MgO igneous clasts (C16, C7, and C27) and one pyroxene crystal (P3), were used for the bulk oxygen isotope analyses at IPGP. Given the amount of material available, the data shown here represent single analyses. Analytical methods are similar to those documented in Rumble *et al.* (*55*). Before analyses, samples were prefluorinated overnight in a BrF_5 atmosphere. Samples were then reacted using laser fluorination, with the released O_2 being purified and analyzed for O isotope compositions using a dual-inlet ion-ratio mass spectrometer (IRMS; Thermo Fisher Delta V). Samples were analyzed along with garnet standard UWG-2 from the Gore Mountain mine, Adirondack Mountains, New York (*56*), and reported versus the international SMOW standard using the conventional delta notation, where $\delta^{18}O = [(^{18}O/^{16}O)_{sample}/(^{18}O/^{16}O)_{standard} - 1] \times 1000$. The typical external errors on $\delta^{18}O$ values are ±0.08‰. The $\Delta^{17}O$ values are expressed as $\Delta^{17}O = \delta^{17}O - [(\delta^{18}O/1000 + 1)^{0.5305} - 1] \times 1000$, with 1 SD values given in data file S4.

SUPPLEMENTARY MATERIALS

REFERENCES AND NOTES

1. A. Udry, G. H. Howarth, C. Herd, J. M. D. Day, T. J. Lapen, What martian meteorites reveal about the interior and surface of Mars. *Earth Space Science Open Archive* **55**, 10.1002/essoar.10503123.1 (2020).
2. L. C. Bouvier, M. M. Costa, J. N. Connelly, N. K. Jensen, D. Wielandt, M. Storey, A. A. Nemchin, M. J. Whitehouse, J. F. Snape, J. J. Bellucci, F. Moynier, A. Agranier, B. Gueguen, M. Schönbächler, M. Bizzarro, Evidence for extremely rapid magma ocean crystallization and crust formation on Mars. *Nature* **558**, 586–589 (2018).
3. M. Humayun, A. Nemchin, B. Zanda, R. H. Hewins, M. Grange, A. Kennedy, J.-P. Lorand, C. Göpel, C. Fieni, S. Pont, D. Deldicque, Origin and age of the earliest Martian crust from meteorite NWA 7533. *Nature* **503**, 513–516 (2013).
4. C. B. Agee, N. V. Wilson, F. M. McCubbin, K. Ziegler, V. J. Polyak, Z. D. Sharp, Y. Asmerom, M. H. Nunn, R. Shaheen, M. H. Thiemens, A. Steele, M. L. Fogel, R. Bowden, M. Glamoclija, Z. Zhang, S. M. Elardo, Unique meteorite from early Amazonian Mars: Water-rich basaltic breccia Northwest Africa 7034. *Science* **339**, 780–785 (2013).
5. I. S. E. Carmichael, The redox states of basic and silicic magmas: A reflection of their source regions? *Contrib. Mineral. Petrol.* **106**, 129–141 (1991).
6. K. Righter, S. R. Sutton, L. Danielson, K. Pando, M. Newville, Redox variations in the inner solar system with new constraints from vanadium XANES in spinels. *Am. Mineral.* **101**, 1928–1942 (2016).
7. C. D. K. Herd, J. J. Papike, A. J. Brearley, Oxygen fugacity of martian basalts from electron microprobe oxygen and TEM-EELS analyses of Fe-Ti oxides. *Am. Mineral.* **86**, 1015–1024 (2001).
8. A. R. Santos, C. B. Agee, F. M. McCubbin, C. K. Shearer, P. V. Burger, R. Tartèse, M. Anand, Petrology of igneous clasts in Northwest Africa 7034: Implications for the petrologic diversity of the martian crust. *Geochim. Cosmochim. Acta* **157**, 56–85 (2015).
9. J. Tuff, J. Wade, B. J. Wood, Volcanism on Mars controlled by early oxidation of the upper mantle. *Nature* **498**, 342–345 (2013).
10. M.-A. Millet, N. Dauphas, N. D. Greber, K. W. Burton, C. W. Dale, B. Debret, C. G. Macpherson, G. M. Nowell, H. M. Williams, Titanium stable isotope investigation of magmatic processes on the Earth and Moon. *Earth Planet. Sci. Lett.* **449**, 197–205 (2016).
11. Z. Deng, M. Chaussidon, P. Savage, F. Robert, R. Pik, F. Moynier, Titanium isotopes as a tracer for the plume or island arc affinity of felsic rocks. *Proc. Natl. Acad. Sci. U.S.A.* **116**, 1132–1135 (2019).
12. F. Farges, G. E. Brown Jr., Coordination chemistry of titanium (IV) in silicate glasses and melts: IV. XANES studies of synthetic and natural volcanic glasses and tektites at ambient temperature and pressure. *Geochim. Cosmochim. Acta* **61**, 1863–1870 (1997).
13. A. C. Johnson, S. M. Aarons, N. Dauphas, N. X. Nie, H. Zeng, R. T. Helz, S. J. Romaniello, A. D. Anbar, Titanium isotopic fractionation in Kilauea Iki lava lake driven by oxide crystallization. *Geochim. Cosmochim. Acta* **264**, 180–190 (2019).
14. L. Hoare, M. Klaver, N. S. Saji, J. Gillies, I. J. Parkinson, C. J. Lissenberg, M.-A. Millet, Melt chemistry and redox conditions control titanium isotope fractionation during magmatic differentiation. *Geochim. Cosmochim. Acta* **282**, 38–54 (2020).
15. X. Zhao, S. Tang, J. Li, H. Wang, R. Helz, B. Marsh, X. Zhu, H. Zhang, Titanium isotopic fractionation during magmatic differentiation. *Contrib. Mineral. Petrol.* **175**, 67 (2020).
16. Supplementary text in the Supplementary Materials file.
17. R. Arató, A. Audétat, FeTiMM – A new oxybarometer for mafic to felsic magmas. *Geochem. Perspect. Lett.* **5**, 19–23 (2017).
18. M. J. Toplis, M. R. Carroll, An experimental study of the influence of oxygen fugacity on Fe-Ti oxide stability, phase relations, and mineral—Melt equilibria in ferro-basaltic systems. *J. Petrol.* **36**, 1137–1170 (1995).
19. H. Y. McSween Jr., G. J. Taylor, M. B. Wyatt, Elemental composition of the martian crust. *Science* **324**, 736–739 (2009).
20. W. V. Boynton, G. J. Taylor, L. G. Evans, R. C. Reedy, R. Starr, D. M. Janes, K. E. Kerry, D. M. Drake, K. J. Kim, R. M. S. Williams, M. K. Crombie, J. M. Dohm, V. Baker, A. E. Metzger, S. Karunatillake, J. M. Keller, H. E. Newsom, J. R. Arnold, J. Brückner, P. A. J. Englert, O. Gasnault, A. L. Sprague, I. Mitrofanov, S. W. Squyres, J. I. Trombka, L. d'Uston, H. Wänke, D. K. Hamara, Concentration of H, Si, Cl, K, Fe, and Th in the low- and mid-latitude regions of Mars. *J. Geophys. Res. Planets* **112**, E12S99 (2007).
21. R. Gellert, R. Rieder, J. Brückner, B. C. Clark, G. Dreibus, G. Klingelhöfer, G. Lugmair, D. W. Ming, H. Wänke, A. Yen, J. Zipfel, S. W. Squyres, Alpha particle x-ray spectrometer (APXS): Results from Gusev crater and calibration report. *J. Geophys. Res. Planets* **111**, E02S05 (2006).
22. D. W. Ming, R. Gellert, R. V. Morris, R. E. Arvidson, J. Brückner, B. C. Clark, B. A. Cohen, C. d'Uston, T. Economou, I. Fleischer, G. Klingelhöfer, T. J. McCoy, D. W. Mittlefehldt, M. E. Schmidt, C. Schröder, S. W. Squyres, E. Tréguier, A. S. Yen, J. Zipfel, Geochemical properties of rocks and soils in Gusev Crater, Mars: Results of the alpha particle x-ray spectrometer from Cumberland Ridge to Home Plate. *J. Geophys. Res. Planets* **113**, E12S39 (2008).
23. M. E. Schmidt, J. L. Campbell, R. Gellert, G. M. Perrett, A. H. Treiman, D. L. Blaney, A. Olilla, F. J. Calef III, L. Edgar, B. E. Elliott, J. Grotzinger, J. Hurowitz, P. L. King, M. E. Minitti, V. Sautter, K. Stack, J. A. Berger, J. C. Bridges, B. L. Ehlmann, O. Forni, L. A. Leshin, K. W. Lewis, S. M. McLennan, D. W. Ming, H. Newsom, I. Pradler, S. W. Squyres, E. M. Stolper, L. Thompson, S. VanBommel, R. C. Wiens, Geochemical diversity in first rocks examined by the Curiosity Rover in Gale Crater: Evidence for and significance of an alkali and volatile-rich igneous source. *J. Geophys. Res. Planets* **119**, 64–81 (2014).
24. A. Cousin, V. Sautter, V. Payré, O. Forni, N. Mangold, O. Gasnault, L. Le Deit, J. Johnson, S. Maurice, M. Salvatore, R. C. Wiens, P. Gasda, W. Rapin, Classification of igneous rocks analyzed by ChemCam at Gale crater, Mars. *Icarus* **288**, 265–283 (2017).
25. K. Lodders, A survey of shergottite, nakhlite and chassigny meteorites whole-rock compositions. *Meteorit. Planet. Sci.* **33**, A183–A190 (1998).
26. J. Filiberto, Geochemistry of Martian basalts with constraints on magma genesis. *Chem. Geol.* **466**, 1–14 (2017).

27. A. Udry, N. G. Lunning, H. Y. McSween Jr., R. J. Bodnar, Petrogenesis of a vitrophyre in the martian meteorite breccia NWA 7034. *Geochim. Cosmochim. Acta* **141**, 281–293 (2014).

28. S. Goderis, A. D. Brandon, B. Mayer, M. Humayun, Ancient impactor components preserved and reworked in martian regolith breccia Northwest Africa 7034. *Geochim. Cosmochim. Acta* **191**, 203–215 (2016).

29. R. H. Hewins, B. Zanda, M. Humayun, A. Nemchin, J.-P. Lorand, S. Pont, D. Deldicque, J. J. Bellucci, P. Beck, H. Leroux, M. Marinova, L. Remusat, C. Göpel, E. Lewin, M. Grange, A. Kennedy, M. J. Whitehouse, Regolith breccia Northwest Africa 7533: Mineralogy and petrology with implications for early Mars. *Meteorit. Planet. Sci.* **52**, 89–124 (2017).

30. F. M. McCubbin, J. W. Boyce, T. Novák-Szabó, A. R. Santos, R. Tartèse, N. Muttik, G. Domokos, J. Vazquez, L. P. Keller, D. E. Moser, D. J. Jerolmack, C. K. Shearer, A. Steele, S. M. Elardo, Z. Rahman, M. Anand, T. Delhaye, C. B. Agee, Geologic history of Martian regolith breccia Northwest Africa 7034: Evidence for hydrothermal activity and lithologic diversity in the Martian crust. *J. Geophys. Res. Planets* **121**, 2120–2149 (2016).

31. R. M. G. Armytage, V. Debaille, A. D. Brandon, C. B. Agee, A complex history of silicate differentiation of Mars from Nd and Hf isotopes in crustal breccia NWA 7034. *Earth Planet. Sci. Lett.* **502**, 274–283 (2018).

32. N. K. Jensen, M. M. Costa, J. N. Connelly, M. Bizzarro, Formation of basalt on Mars at ~4443 Ma by impact melting of the primordial crust. *Goldschmidt 2020 abstr.* 1361 (2020); http://goldschmidtabstracts.info/2020/1361.pdf.

33. S. Hu, Y. Lin, J. Zhang, J. Hao, W. Xing, T. Zhang, W. Yang, H. Changela, Ancient geologic events on Mars revealed by zircons and apatites from the Martian regolith breccia NWA 7034. *Meteorit. Planet. Sci.* **54**, 850–879 (2019).

34. N. D. Greber, N. Dauphas, I. S. Puchtel, B. A. Hofmann, N. T. Arndt, Titanium stable isotopic variations in chondrites, achondrites and lunar rocks. *Geochim. Cosmochim. Acta* **213**, 534–552 (2017).

35. Z. Deng, F. Moynier, P. A. Sossi, M. Chaussidon, Bridging the depleted MORB mantle and the continental crust using titanium isotopes. *Geochem. Perspect. Lett.* **9**, 11–15 (2018).

36. Z. Deng, F. Moynier, K. van Zuilen, P. A. Sossi, E. A. Pringle, M. Chaussidon, Lack of resolvable titanium stable isotopic variations in bulk chondrites. *Geochim. Cosmochim. Acta* **239**, 409–419 (2018).

37. J. M. Brenan, N. R. Bennett, Z. Zajacz, Experimental results on fractionation of the highly siderophile elements (HSE) at variable pressures and temperatures during planetary and magmatic differentiation. *Rev. Mineral. Geochem.* **81**, 1–87 (2016).

38. M. J. Toplis, A. Corgne, An experimental study of element partitioning between magnetite, clinopyroxene and iron-bearing silicate liquids with particular emphasis on vanadium. *Contrib. Mineral. Petrol.* **144**, 22–37 (2002).

39. W. F. McDonough, S.-s. Sun, The composition of the Earth. *Chem. Geol.* **120**, 223–253 (1995).

40. K. Ziegler, Z. D. Sharp, C. B. Agee, The unique NWA 7034 martian meteorite: Evidence for multiple oxygen isotope reservoirs (44th Lunar and Planetary Science Conference, 2013).

41. A. Ali, I. Jabeen, D. Gregory, R. Verish, N. R. Banerjee, New triple oxygen isotope data of bulk and separated fractions from SNC meteorites: Evidence for mantle homogeneity of Mars. *Meteorit. Planet. Sci.* **51**, 981–995 (2016).

42. A. A. Nemchin, M. Humayun, M. J. Whitehouse, R. H. Hewins, J.-P. Lorand, A. Kennedy, M. Grange, B. Zanda, C. Fieni, D. Deldicque, Record of the ancient martian hydrosphere and atmosphere preserved in zircon from a martian meteorite. *Nat. Geosci.* **7**, 638–642 (2014).

43. D. J. Cherniak, X. Y. Zhang, M. Nakamura, E. B. Watson, Oxygen diffusion in monazite. *Earth Planet. Sci. Lett.* **226**, 161–174 (2004).

44. R. N. Clayton, T. K. Mayeda, Oxygen isotope studies of carbonaceous chondrites. *Geochim. Cosmochim. Acta* **63**, 2089–2104 (1999).

45. J. J. Bellucci, M. J. Whitehouse, A. A. Nemchin, J. F. Snape, G. G. Kenny, R. E. Merle, P. A. Bland, G. K. Benedix, Tracing martian surface interactions with the triple O isotope compositions of meteoritic phosphates. *Earth Planet. Sci. Lett.* **531**, 115977 (2020).

46. P. Lognonné, W. B. Banerdt, W. T. Pike, D. Giardini, U. Christensen, R. F. Garcia, T. Kawamura, S. Kedar, B. Knapmeyer-Endrun, L. Margerin, F. Nimmo, M. Panning, B. Tauzin, J.-R. Scholz, D. Antonangeli, S. Barkaoui, E. Beucler, F. Bissig, N. Brinkman, M. Calvet, S. Ceylan, C. Charalambous, P. Davis, M. van Driel, M. Drilleau, L. Fayon, R. Joshi, B. Kenda, A. Khan, M. Knapmeyer, V. Lekic, J. McClean, D. Mimoun, N. Murdoch, L. Pan, C. Perrin, B. Pinot, L. Pou, S. Menina, S. Rodriguez, C. Schmelzbach, N. Schmerr, D. Sollberger, A. Spiga, S. Stähler, A. Stott, E. Stutzmann, S. Tharimena, R. Widmer-Schnidrig, F. Andersson, V. Ansan, C. Beghein, M. Böse, E. Bozdag, J. Clinton, I. Daubar, P. Delage, N. Fuji, M. Golombek, M. Grott, A. Horleston, K. Hurst, J. Irving, A. Jacob, J. Knollenberg, S. Krasner, C. Krause, R. Lorenz, C. Michaut, R. Myhill, T. Nissen-Meyer, J. ten Pierick, A. C. Plesa, C. Quantin-Nataf, J. Robertsson, L. Rochas, M. Schimmel, S. Smrekar, T. Spohn, N. Teanby, J. Tromp, J. Vallade, N. Verdier, C. Vrettos, R. Weber, D. Banfield, E. Barrett, M. Bierwirth, S. Calcutt, N. Compaire, C. L. Johnson, D. Mance, F. Euchner, L. Kerjean, G. Mainsant, A. Mocquet, J. A. Rodriguez Manfredi, G. Pont, P. Laudet, T. Nebut, S. de Raucourt, O. Robert, C. T. Russell, A. Sylvestre-Baron, S. Tillier, T. Warren, M. Wieczorek, C. Yana, P. Zweifel, Constraints on the shallow elastic and anelastic structure of Mars from Insight seismic data. *Nat. Geosci.* **13**, 213–220 (2020).

47. M. Turbet, C. Gillmann, F. Forget, B. Baudin, A. Palumbo, J. Head, O. Karatekin, The environmental effects of very large bolide impacts on early Mars explored with a hierarchy of numerical models. *Icarus* **335**, 113419 (2020).

48. R. M. Haberle, K. Zahnle, N. G. Barlow, K. E. Steakley, Impact degassing of H_2 on early Mars and its effect on the climate system. *Geophys. Res. Lett.* **46**, 13355–13362 (2019).

49. R. D. Wordsworth, The climate of early Mars. *Annu. Rev. Earth Planet. Sci.* **44**, 381–408 (2016).

50. R. M. Ramirez, R. Kopparapu, M. E. Zugger, T. D. Robinson, R. Freedman, J. F. Kasting, Warming early Mars with CO_2 and H_2. *Nat. Geosci.* **7**, 59–63 (2014).

51. R. Y. Wordsworth, Y. Kalugina, S. Lokshtanov, A. Vigasin, B. Ehlmann, J. Head, C. Sanders, H. Wang, Transient reducing greenhouse warming on early Mars. *Geophys. Res. Lett.* **44**, 665–671 (2017).

52. R. M. Ramirez, R. A. Craddock, T. Usui, Climate simulations of early Mars with estimated precipitation, runoff, and erosion rates. *J. Geophys. Res. Planets* **125**, e2019JE006160 (2020).

53. A. Kamada, T. Kuroda, Y. Kasaba, N. Terada, H. Nakagawa, K. Toriumi, A coupled atmosphere–hydrosphere global climate model of early Mars: A 'cool and wet' scenario for the formation of water channels. *Icarus* **338**, 113567 (2020).

54. J. B. Creech, B. Paul, Isospike: Improved double-spike inversion software. *Geostand. Geoanalytical Res.* **39**, 7–15 (2014).

55. D. Rumble III, J. Farquhar, E. D. Young, C. P. Christensen, In situ oxygen isotope analysis with an excimer laser using F_2 and BrF_5 reagents and O_2 gas as analyte. *Geochim. Cosmochim. Acta* **61**, 4229–4234 (1997).

56. J. W. Valley, N. E. Kitchen, M. J. Kohn, C. R. Niendorf, M. J. Spicuzza, UWG-2, a garnet standard for oxygen isotope ratios: Strategies for high precision and accuracy with laser heating. *Geochim. Cosmochim. Acta* **59**, 5223–5231 (1995).

57. G. Mallmann, H. St C. O'Neill, The effect of oxygen fugacity on the partitioning of Re between crystals and silicate melt during mantle melting. *Geochim. Cosmochim. Acta* **71**, 2837–2857 (2007).

58. M. A. Elburg, V. S. Kamenetsky, J. D. Foden, A. Sobolev, The origin of medium-K ankaramitic arc magmas from Lombok (Sunda arc, Indonesia): Mineral and melt inclusion evidence. *Chem. Geol.* **240**, 260–279 (2007).

59. P. A. Sossi, S. Klemme, H. St C. O'Neil, J. Berndt, F. Moynier, Evaporation of moderately volatile elements from silicate melts: Experiments and theory. *Geochim. Cosmochim. Acta* **260**, 204–231 (2019).

60. W. Wang, S. Huang, S. Huang, X. Zhao, Z. Wu, Equilibrium inter-mineral titanium isotope fractionation: Implication for high-temperature titanium isotope geochemistry. *Geochim. Cosmochim. Acta* **269**, 540–553 (2020).

61. F. Gaillard, B. Scaillet, M. Pichavant, J.-M. Bény, The effect of water and fO_2 on the ferric–ferrous ratio of silicic melts. *Chem. Geol.* **174**, 255–273 (2001).